

Distinguishing Neutrino Mass Hierarchies using Dark Matter Annihilation Signals at IceCube

Rouzbeh Allahverdi ^{a,1}, Bhaskar Dutta ^{b,2}, Dilip Kumar Ghosh ^{c,3}, Bradley Knockel ^{a,4}, Ipsita Saha ^{c,5}

^a *Department of Physics and Astronomy, University of New Mexico, Albuquerque, NM 87131, USA.*

^b *Department of Physics and Astronomy, Mitchell Institute for Fundamental Physics and Astronomy, Texas A & M University, College Station, TX 77843-4242, USA.*

^c *Department of Theoretical Physics, Indian Association for the Cultivation of Science, 2A & 2B, Raja S.C. Mullick Road, Kolkata 700032, India.*

Abstract

We explore the possibility of distinguishing neutrino mass hierarchies through the neutrino signal from dark matter annihilation at neutrino telescopes. We consider a simple extension of the standard model where the neutrino masses and mixing angles are obtained via the type-II seesaw mechanism as an explicit example. We show that future extensions of IceCube neutrino telescope may detect the neutrino signal from DM annihilation at the Galactic Center and inside the Sun, and differentiate between the normal and inverted mass hierarchies, in this model.

1 Introduction

Although various lines of evidence support the existence of dark matter (DM) in the universe, its identity remains as a mystery. Among various proposed candidates, the weakly interacting massive particles (WIMPs) are promising ones that typically arises in many extensions of the standard model (SM) [1, 2]. Major direct, indirect, and collider experimental searches are currently underway to detect the particle nature of DM and determine its properties.

Just like DM, the origin of neutrino mass and mixing defines a very interesting area of investigation beyond the SM (BSM) [3, 4]. These are the two encouraging avenues of new physics and a large number of BSM scenarios have already been proposed to address them. It will be even more interesting to investigate models where the two sectors are connected. In fact, such a connection arises naturally in a class of models where DM is tied to the neutrino sector. For example, in type-II seesaw plus a singlet scalar scenario [5], it has been shown that the neutrino mass hierarchy can influence the DM annihilation rate to charged leptons as well as neutrinos and subsequently provide a possible explanation of the positron fraction excess observed at the AMS-02 experiment [6]. Similar studies have been done in the $B - L$ extension of the minimal supersymmetric standard model (MSSM) where it is shown that the annihilation of the right-handed sneutrino DM produces neutrino final states with a distinct feature [7]. There have been studies on the possibility of discovering the $B - L$ sneutrino

¹rouzbeh@unm.edu

²dutta@physics.tamu.edu

³tpdkg@iacs.res.in

⁴knockel.physics@gmail.com

⁵tpis@iacs.res.in

DM at the LHC [8–10]. The connection between the DM and neutrinos in such scenarios can also be probed through DM direct detection [11] and some indirect detection experiments [12]. Therefore, a combination of direct, indirect and collider signatures could be useful to explore this connection (for a review, see [13]).

Our focus here is on the DM indirect detection signals as a means of testing the connection between the DM and neutrinos. Neutrino telescopes like IceCube are able to examine these models through the signal arising from the DM annihilation into neutrinos at the Galactic Center [14] and inside the Sun [15]. Unlike the photon flux, the neutrino flux arising from the DM annihilation at the Galactic Center has less astrophysical background uncertainty, which allows us to probe the exact nature of the DM more accurately. However, the model prediction for the photon fluxes coming from the DM annihilation at the Galactic Center should be consistent with the Fermi-LAT [16] data on the gamma-ray flux. Therefore, it will be interesting to combine the results from IceCube and Fermi-LAT to study models where the DM and the neutrino sectors are interconnected.

In this paper, we study these issues within the above mentioned extension of the SM [5, 6]. In this model, the light neutrino masses and mixing angles are generated using the well-known type-II seesaw mechanism [17–21] that introduces $SU(2)_L$ triplet scalars. The neutral component of the triplet acquires a non-zero vacuum expectation value (vev) that generates tiny neutrino masses by breaking lepton number by two units and mixing among different neutrino flavors. Among the SM particles, these triplet scalars only couple to gauge bosons through gauge couplings and to leptons via Yukawa couplings. These Yukawa couplings are related to the triplet vev, which in turn determines different decay modes of these triplet scalars. It has been observed [22, 23] that the triplets will dominantly decay to a pair of leptons if the vev is less than 0.1 MeV, otherwise the gauge boson final state will become dominant. In order to accommodate a stable DM candidate, the model is augmented by a SM singlet scalar with a Z_2 symmetry [5]. In the minimal case, the DM only couples to the Higgs and to the triplet scalars. For a vev smaller than 0.1 MeV, the annihilation of the DM produces a pair of triplets that will further decay to SM leptons (including neutrinos) with almost 100% branching fraction. Therefore, the flavor composition of the final states will depend upon the neutrino mass hierarchy that sets the Yukawa couplings. We exploit this feature and show how different neutrino mass hierarchies can be distinguished by using the muon signal arising from conversion of muon neutrinos from DM annihilation at the Galactic Center and inside the Sun at IceCube. We note that the photon signal from the Galactic Center does not discriminate amongst different hierarchies because the difference will not be significant.

The paper is organized as follows. In Sec. 2, we discuss the model in brief. In Sec. 3, we present the analysis of the neutrino signal from DM annihilation at the Galactic Center and inside the Sun for normal and inverted hierarchies. We also calculate the corresponding muon spectra at the detector and compare them with the background. Finally, in Sec. 4 we present our discussion and conclusion.

2 Type-II seesaw with a scalar singlet DM candidate

The minimal version of the type-II seesaw model is an extension of the SM that includes a $SU(2)_L$ scalar triplet Δ with hypercharge $Y = 2$.

$$\Delta = \begin{pmatrix} \frac{\Delta^+}{\sqrt{2}} & \Delta^{++} \\ \Delta^0 & \frac{\Delta^-}{\sqrt{2}} \end{pmatrix} \quad (1)$$

In order to accommodate a cold dark matter (CDM) candidate, we introduce a SM singlet real scalar D . The stability of the DM candidate is ensured by imposing a Z_2 symmetry under which D is odd while all other SM particles and the triplet Δ are even.

The scalar potential of the model, including the relevant terms for the DM candidate D , is given by [6]

$$\begin{aligned}\mathcal{V}(\Phi, \Delta) &= -m_\Phi^2(\Phi^\dagger\Phi) + \frac{\lambda}{2}(\Phi^\dagger\Phi)^2 + M_\Delta^2\text{Tr}(\Delta^\dagger\Delta) + \frac{\lambda_1}{2}\left[\text{Tr}(\Delta^\dagger\Delta)\right]^2 \\ &\quad + \frac{\lambda_2}{2}\left(\left[\text{Tr}(\Delta^\dagger\Delta)\right]^2 - \text{Tr}\left[(\Delta^\dagger\Delta)^2\right]\right) + \lambda_4(\Phi^\dagger\Phi)\text{Tr}(\Delta^\dagger\Delta) \\ &\quad + \lambda_5\Phi^\dagger[\Delta^\dagger, \Delta]\Phi + \left(\frac{\Lambda_6}{\sqrt{2}}\Phi^\text{T}i\sigma_2\Delta^\dagger\Phi + \text{h.c.}\right), \\ \mathcal{V}_{\text{DM}}(\Phi, \Delta, D) &= \frac{1}{2}m_D^2D^2 + \lambda_DD^4 + \lambda_\Phi D^2(\Phi^\dagger\Phi) + \lambda_\Delta D^2\text{Tr}(\Delta^\dagger\Delta).\end{aligned}\tag{2}$$

where Φ is the SM Higgs doublet. The couplings $\lambda_i (i = 1 - 5)$ can be taken as real without any loss of generality. Due to spontaneous symmetry breaking, the non-zero vev of the Higgs doublet generates a tadpole term through interaction involving the Λ_6 coupling in Eq. (2). This in turn induces a non-zero vev (v_Δ) for the neutral component of the triplet thereby breaking lepton number by two units. This triplet vev contributes to the SM gauge boson masses at the tree level which leads to a deviation in the electroweak ρ parameter. Hence, v_Δ is constrained by the electroweak precision data that requires the ρ parameter to be close to the SM value of unity [24] which eventually demands $v_\Delta < 2$ GeV [25]. In addition to this, current experimental bounds on lepton flavor violating processes put a lower bound on v_Δ [26–28] as

$$v_\Delta M_\Delta \geq 150 \text{ eV GeV}.\tag{4}$$

It is to be mentioned here that we assume negligible mixing between the doublet and triplet scalars in our analysis⁶ and with this assumption, the DM potential of Eq. (3) can be expressed in terms of physical scalars ($h, H^\pm, H^{\pm\pm}, H^0, A^0$) as

$$\begin{aligned}\mathcal{V}_{\text{DM}}(\Phi, \Delta, D) &= \frac{1}{2}m_{DM}^2D^2 + \lambda_DD^4 + \lambda_\Phi vD^2h + \frac{1}{2}\lambda_\Phi D^2h^2 + \\ &\quad \lambda_\Delta D^2\left[H^{++}H^{--} + H^+H^- + \frac{1}{2}(H_0^2 + A_0^2) + \frac{1}{2}v_\Delta H_0\right].\end{aligned}\tag{5}$$

Here, $m_{DM}^2 = m_D^2 + \lambda_\Phi v^2 + \lambda_\Delta v_\Delta^2$ denotes the physical mass of the DM candidate. It is evident from Eq. (5) that the DM candidate can annihilate to a pair of Higgs and to a pair of exotic triplet scalar particles through the coupling parameters λ_Φ and λ_Δ . In the limit $m_{DM} > m_\Delta$, where, m_Δ is the degenerate mass of all triplet scalars, the annihilation cross section of the DM candidate (non-relativistic) is expressed as

$$\langle\sigma v\rangle = \frac{1}{16\pi m_{DM}^2}\left[\lambda_\phi^2\left(1 - \frac{m_h^2}{m_{DM}^2}\right) + 6\lambda_\Delta^2\left(1 - \frac{m_\Delta^2}{m_{DM}^2}\right)\right].\tag{6}$$

This should yield the correct relic abundance of the DM particle that lies within the 3σ limit of current Planck bound $\Omega_{DM}h^2 = 0.1199 \pm 0.0027$ [30]. Now, the final state of DM annihilation will depend upon the branching fraction of the Higgs and the triplet scalar decay. The triplet scalars can couple to the SM gauge bosons through gauge coupling and to SM lepton doublets through Yukawa couplings.

$$\mathcal{L}_Y = \mathcal{L}_Y^{\text{SM}} - \frac{1}{\sqrt{2}}(Y_\Delta)_{ij}L_i^\text{T}Ci\sigma_2\Delta L_j + \text{h.c.}\tag{7}$$

⁶Detailed expressions for physical scalar mass eigenstates can be found in [29].

Here, C is the charge conjugation operator and $L_i = (\nu_i, \ell_i)_L^T$ is the $SU(2)_L$ lepton doublet with i being the three generation indices. Further, these Yukawa couplings can be obtained from the Majorana mass matrix of neutrinos that arises due to the non-zero triplet vev v_Δ .

$$(M_\nu)_{ij} = v_\Delta (Y_\Delta)_{ij}, \quad (8)$$

$$Y_\Delta = \frac{M_\nu}{v_\Delta} = \frac{1}{v_\Delta} U^\top M_\nu^{\text{diag}} U, \quad (9)$$

where $M_\nu^{\text{diag}} = \text{diag}(m_1, m_2, m_3)$ and U is the PMNS mixing matrix.

With the recent global analysis data (see Eq. (18) in the Appendix), and after using Eq. (9), we obtain the following structure of the Yukawa coupling matrix for the normal hierarchy (NH) and inverted hierarchy (IH) scenarios

$$Y_\Delta = \frac{10^{-2} \text{ eV}}{v_\Delta} \times \begin{cases} \begin{pmatrix} 1.08 - 0.29i & -1.55 + 0.09i & 1.23 - 0.31i \\ -1.55 + 0.09i & 2.07 + 0.26i & -1.59 - 0.21i \\ 1.23 - 0.31i & -1.59 - 0.21i & 2.59 + 0.0i \end{pmatrix} & \text{(normal hierarchy)} \\ \begin{pmatrix} 3.84 + 0.34i & 1.21 - 0.13i & -1.39 - 0.94i \\ 1.21 - 0.13i & 2.97 - 0.35i & 1.98 - 0.65i \\ -1.39 - 0.94i & 1.98 - 0.65i & 2.66 + 0.01i \end{pmatrix} & \text{(inverted hierarchy)}. \end{cases} \quad (10)$$

To find the Yukawa matrix for the degenerate case, we impose the 95% C.L. limit on the sum of all light neutrino masses $\sum_i m_i < 0.23 \text{ eV}$ from Planck [30], which uses the Baryon Acoustic Oscillation (BAO) and Cosmic Microwave Background (CMB) data. By choosing $m_1 \simeq m_2 \simeq m_3 = 0.07 \text{ eV}$, we find

$$Y_\Delta = \frac{10^{-2} \text{ eV}}{v_\Delta} \times \begin{pmatrix} 6.80 - 0.06i & -0.13 - 0.04i & 0. - 1.65i \\ -0.13 - 0.04i & 6.91 - 0.03i & 0. - 1.10i \\ 0. - 1.65i & 0. - 1.10i & 6.71 + 0.10i \end{pmatrix} \quad \text{(degenerate case)}. \quad (11)$$

However, as we will see later, the degenerate scenario does not offer any significant information in our study.

The triplet scalar decay to leptonic final states, $H^{++} \rightarrow \ell^+ \ell^+$, $H^+ \rightarrow \ell^+ \nu_\ell$, $H_0/A_0 \rightarrow \nu \nu$ with almost 100% branching ratio when $v_\Delta \leq 0.1 \text{ MeV}$. On the other hand, for larger $v_\Delta (> 0.1 \text{ MeV})$, gauge boson final states become dominant with the decay modes $H^{++} \rightarrow W^+ W^+$, $H^+ \rightarrow W^+ Z$, $H_0/A_0 \rightarrow ZZ/W^+ W^-$ ⁷. For almost same order of λ_ϕ and λ_Δ within the range for producing correct relic density, the DM can annihilate to three different final states (depending upon the branching ratios i.e on v_Δ for triplets) :

- (i) neutrino and charged lepton final states.
- (ii) $W^\pm W^\mp$, ZZ final states mainly from triplet scalar decays; WW^* , ZZ^* final states arise from the decay of the SM Higgs boson.
- (iii) b, τ final states from the decay of the SM Higgs boson.

We choose two extreme values of v_Δ , namely, 1 eV and 1 GeV, respectively to incorporate the effect of triplet scalars decay to only leptonic final state or only to non-leptonic final states. Our study is mainly focused on the study of neutrino flux coming from DM annihilation which can be obtained from all the above three final states. However, for triplet scalars decaying into leptonic final states includes

⁷Throughout this analysis we assume degenerate triplet scalars.

the contribution of Yukawa couplings Y_Δ which is a function of neutrino mass hierarchy and we expect to see the difference in the neutrino flux between the NH and IH scenarios. In the following sections, we will explicitly show how our analysis depends upon the neutrino mass hierarchy.

In this regard, it is to be noted that the triplet scalars can produce interesting signals at the colliders. The strongest limit on the scalar masses comes from the current searches at the LHC for the signature of doubly charged scalar where they can be pair produced via Drell-Yan and Vector Boson fusion and then decay to a pair of same-sign leptons. The experimental lower bound on $m_{H^{\pm\pm}}$ has been set by the ATLAS experiment [31] from a pair of isolated lepton search for $(H^{\pm\pm} \rightarrow e^\pm e^\pm)$ and $(H^{\pm\pm} \rightarrow \mu^\pm \mu^\pm)$ decay modes at the center of mass energy 8 TeV. The 95% C.L. lower limit on the doubly charged Higgs mass for the same-sign isolated muons final state exclude mass range below 516 GeV. However, the experimental lower limit is based on the assumption that the doubly charged scalar decay to the dimuon channel with 100% branching ratio which is not the case in our scenario. In this model, the doubly charged scalar decay to dimuon channel with atmost 30% branching ratio and thus the lower limit on $m_{H^{\pm\pm}}$ can be relaxed. Following Fig. 5 of Reference [31], we set the degenerate mass of the triplets (m_Δ) as 400 GeV throughout our analysis.

3 Analysis

In this section, we demonstrate our findings on the DM annihilation at the Galactic Center and inside the Sun and the possibilities of using the respective neutrino signals to distinguish the NH and IH scenarios. For the purpose of our analysis, we choose to work with four benchmark points, shown in Table 1, by fixing v_Δ for two DM masses. We choose the DM mass to be greater than 400 GeV to get on-shell triplet scalars in the pair production processes of DM annihilation. Our choice of v_Δ has already been justified in the previous section. We choose λ_Δ and λ_Φ couplings in the model (see Eq. (3)) such that the correct DM abundance is obtained via thermal freeze-out with nominal value for thermally averaged annihilation cross-section $\langle\sigma_{\text{ann}}v\rangle \simeq 3 \times 10^{-26} \text{ cm}^3/\text{s}$. λ_Φ also enters into the direct detection cross section (σ_{SI}) through the t -channel exchange of the SM Higgs. Values of λ_Φ that satisfy thermal relic abundance yield a direct detection cross section well below the current limits from LUX experiment [32]. The choice of λ_Δ and λ_Φ and the corresponding relic density and direct detection cross section are also listed in Table 1. The correct DM relic abundance can also be produced via non-thermal mechanisms [33–35] in which case a larger DM annihilation cross section is allowed. We will discuss the implications of a larger annihilation cross section at the end of this section.

As mentioned earlier, the DM annihilation will give rise to neutrino fluxes of different flavors that will help in distinguishing the structure of Yukawa coupling and, hence, the neutrino mass hierarchy. The IceCube detects neutrinos by recording the Cherenkov light from relativistic charged particles in its volume. Muon neutrinos (ν_μ) produce muon (μ) tracks via the charged current interactions in the detector. On the other hand, electron neutrinos (ν_e) and tau neutrinos (ν_τ) result in hadronic and electromagnetic cascade events in the ice. Since the cascades are localized, they carry no directional information, and hence are not good enough for performing a meaningful DM search over the background. For this reason, we focus on ν_μ fluxes that arrive on the Earth. We also estimate the photon flux for all scenarios in our model. Cosmic ray showers create a muon background that can be controlled by selecting only the upward going events since muons are stopped in the Earth. This limits the observation of DM signal to the time when the source is below the horizon. With atmospheric muons thus eliminated, the most significant contribution to the remaining background comes from atmospheric neutrinos [36]. In addition to this, a portion of the detector may be used as a veto to observe the contained muon events with a conversion vertex inside the instrumented volume, as in the case of DeepCore array in IceCube. The veto procedure virtually eliminates the contribution to the

| Benchmarks | v_Δ | $m_{\text{DM}}(\text{GeV})$ | $m_\Delta(\text{GeV})$ | λ_Δ | λ_ϕ | relic density | $\sigma_{SI} \text{ (pb)}$ |
|------------|------------|-----------------------------|------------------------|------------------|----------------|---------------|----------------------------|
| BP1 | 1 eV | 500 | 400 | 0.055 | 0.04 | 0.117 | 2.25×10^{-10} |
| BP2 | 1 eV | 700 | 400 | 0.075 | 0.05 | 0.122 | 1.79×10^{-10} |
| BP3 | 1 GeV | 500 | 400 | 0.055 | 0.04 | 0.117 | 2.25×10^{-10} |
| BP4 | 1 GeV | 700 | 400 | 0.075 | 0.05 | 0.122 | 1.79×10^{-10} |

Table 1: Benchmark Points (BPs) and the corresponding DM relic density and direct detection cross-sections.

background from atmospheric muons by selecting only contained vertices. This increases the potential observation time to the full year when the source is both above and below the horizon.

We use both contained and through-going muons in our analysis. For contained muon tracks, the vertex at which ν_μ is converted to a muon, is within the detector volume. Through-going muons represent those events that go through a surface inside the detector but may have been produced outside it. To acquire the muon spectra, we use three simple methods:

1. WimpSim [37] automatically provides muons converted from solar neutrinos.
2. DarkSUSY [38] gives muons from atmospheric neutrinos (which we average to make an isotropic approximation).
3. Finally, GENIE [39] provides muons converted from neutrinos coming from the Galactic Center.

GENIE provides the spectrum of contained muons produced from ν_μ s arriving at the detector. To find the total number of muon events, we use the total deep-inelastic charged-current cross sections from reference [40] to find the average ν_μ -to- μ and $\bar{\nu}_\mu$ -to- $\bar{\mu}$ cross sections. Modeling the Galactic Center as an isotropic circle with radius of 5° and ignoring detector angular resolution, we obtain a 5° optimal cut, whereas the solar muons have a 2° optimal cut. To find the through-going muons, we propagate the muons using the parameters of Table (4) of reference [41].

In order to generate the energy spectra of the SM particles that are produced at the annihilation point, we first create the model file for CalcHEP using FeynRules 2.0 [42] and then use CalcHEP 3.6.23 [43] and Pythia-6 [44] to get the spectra. These spectra are valid both at the Galactic Center and inside the Sun. In the following we present our result for these two distinct DM annihilation points.

3.1 Signals from DM annihilation in the Galactic Center

To calculate the fluxes near the Galactic Center, we run the indirect detection module of micrOMEGAsv4.1.8 [45] and measure the fluxes for angle of sight $0^\circ \leq \Psi \leq 5^\circ$. We use the Navarro-Frenk-White (NFW) [46] profile $\rho(r) = \rho_0(r/r_s)^{-1}/(1+r/r_s)^2$ with $r_s = 20 \text{ kpc}$, $\rho_0 = 0.4 \text{ GeV/cm}^3$. It is noteworthy that if the annihilation of our proposed DM candidate happens near the Galactic Center, then the final state neutrinos will encounter oscillations on their way to the Earth. In the Appendix, we show the flavor dependent probability of neutrino flux that originates at the Galactic Center and reaches the detector surface on the Earth. Hence, the final neutrino fluxes will be given by Eq.(16-19b). We have checked that varying all neutrino oscillation parameters within the 3σ allowed range about their best fit central value results in $\mathcal{O}(3 - 4\%)$ change in the neutrino flux from DM annihilation at the Galactic Center. This is much smaller than the difference due to different mass hierarchies.

Following are the interesting features that are seen in Figs. 1, 2 and 3.

- Fig. 1 displays the ν_μ fluxes for NH and IH for BP1 and BP2 which is for $v_\Delta = 1$ eV. As previously argued, at such low vev, the triplet scalars generate leptonic final state with almost 100% branching ratio and the DM annihilation to two on-shell triplet scalars mainly contribute to the annihilation cross section, hence to the ν_μ flux. Now, it is to be observed that for $m_{\text{DM}} = 500$ GeV, the flux rises at around 100 GeV and then falls near 400 GeV and similarly, the rise and fall occur at 60 GeV and 640 GeV for $m_{\text{DM}} = 700$ GeV. This is not surprising and can be understood by the kinematics of the DM annihilation. The triplets are produced on-shell with some boost that comes from the mass difference between the DM and the triplets. Thus the two-body final states render a box like feature with end points $m_{\text{DM}}(1 \pm \beta)/2$ where $\beta = \sqrt{1 - m_\Delta^2/m_{\text{DM}}^2}$.
- We also see from Fig. 1 that there exists a significant difference between the NH and the IH scenarios. This is due to the fact that in the NH case, we get more taus (τ) from the triplet decays which produces ν_τ and the ν_τ further gets converted into ν_μ . For both the DM mass, the neutrino flux can be easily a factor of two higher in the NH scenario than the IH case. The neutrino flux due to degenerate case will be in between the flux generated for NH and IH cases. This is simply because in the degenerate case, we get less τ s from the triplet decays compared to the NH case but more than the IH case. This is true for all our discussions to follow. Therefore, the degenerate case will not provide any new insight and so we restrain ourselves from doing any further remark on this case.

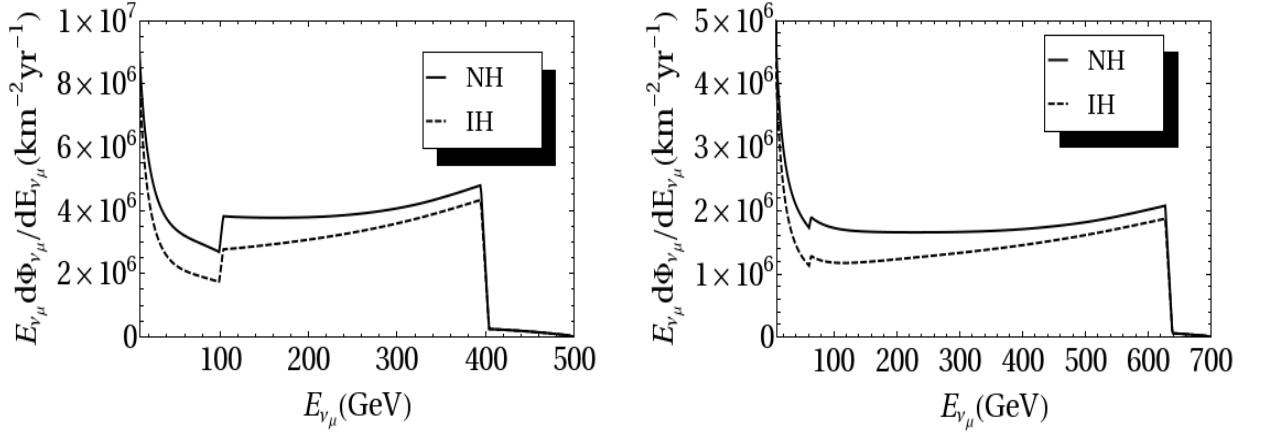


Figure 1: Spectra of ν_μ from DM annihilation at the Galactic Center for BP1 (left) with $m_{\text{DM}} = 500$ GeV and BP2 (right) with $m_{\text{DM}} = 700$ GeV.

- In Fig. 2, we present the diffused photon fluxes for NH and IH cases. In our model, the photon flux arises from external charged lepton legs, final state radiation, and secondary decay of charged leptons that are directly produced from triplet decay. For both the benchmark points, we observe that the photon flux does not distinguish between NH and IH cases ⁸.
- With the increase in v_Δ , the branching ratio of the triplet scalars to leptons reduces and the decay modes with gauge boson final states open up and at sufficiently large v_Δ , $\text{BR}(H^{\pm\pm} \rightarrow W^\pm W^\pm) \simeq 100\%$, dominating over the leptonic final states. Hence, for $v_\Delta = 1$ GeV, the dependence on neutrino mass hierarchy gets washed away. Moreover, the contribution to neutrino fluxes coming

⁸The DM annihilation can also produce photon lines via charged scalar loop processes $\text{DM} + \text{DM} \rightarrow \gamma\gamma$ and $\text{DM} + \text{DM} \rightarrow Z\gamma$ with respective energies m_{DM} and $m_{\text{DM}}(1 - \frac{m_Z^2}{m_{\text{DM}}^2})$. However, the line signal is highly suppressed relative to the diffused photon signal in our model, which is in agreement with the fact that Fermi-LAT has not observed any photon line at such energies.

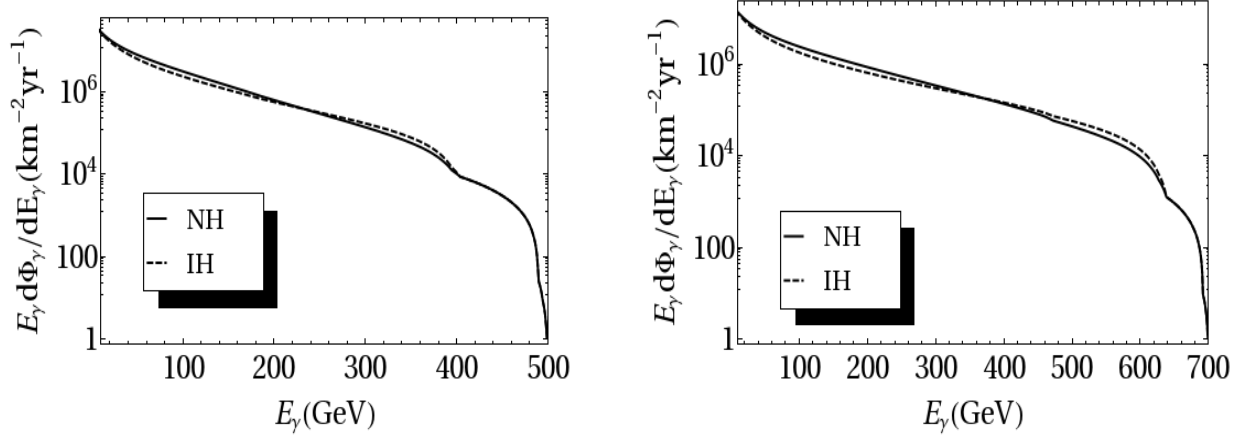


Figure 2: Photon spectra from DM annihilation at the Galactic Center for BP1 (left) with $m_{\text{DM}} = 500$ GeV and BP2 (right) with $m_{\text{DM}} = 700$ GeV.

from DM annihilating to Higgs will become more pronounced in this case. In Fig. 3, we show neutrino fluxes for BP3 and BP4 and evidently these do not distinguish between NH and IH cases. However, the shapes of neutrino spectra are different compared to the previous $v_\Delta = 1$ eV cases as shown in the Fig. 1. As expected, the flux is higher in the previous case because the leptonic final states originate from direct triplet decay. The photon flux, however, does not draw any discrimination between $v_\Delta = 1$ eV and 1 GeV cases or between NH and IH scenarios.

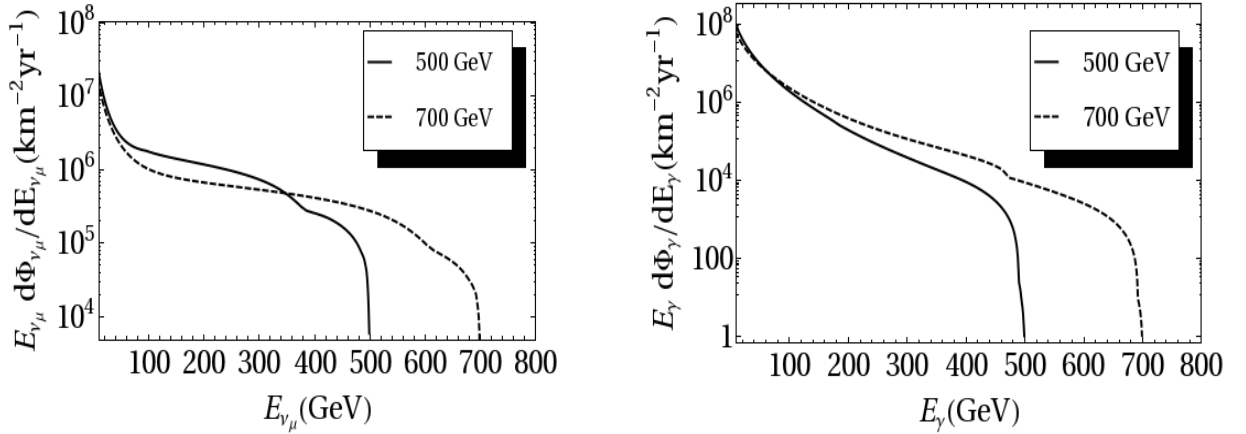


Figure 3: Spectra of ν_μ (left) and Photon (right) from DM annihilation at the Galactic Center for BP3 and BP4.

3.2 Signals from DM annihilations inside the Sun

DM particles that pass through the Sun lose energy due to the DM-nucleon scattering and get gravitationally trapped [47–53]. The total rate of DM annihilations Γ_{ann} inside the Sun follows [1]

$$\Gamma_{\text{ann}} = \frac{C}{2} \tanh^2(\sqrt{CA}t). \quad (12)$$

Here C is the capture rate of DM particles by the Sun, which is related to σ_{SI} in our model, and A is related to the DM annihilation cross section σ_{ann} (for details, see [1]). DM capture and annihilation

reach equilibrium when $t > \tau_{\text{eq}} \equiv (\sqrt{CA})^{-1}$, in which case $\Gamma_{\text{ann}} \approx C/2$. For values of σ_{SI} given in Table 1, and $\langle \sigma_{\text{ann}} v \rangle = 3 \times 10^{-26} \text{ cm}^3 \text{ s}^{-1}$, the equilibrium condition is achieved for the age of the Sun. We note that as long as equilibrium is established, the total rate of DM annihilations is controlled by the direct detection cross section σ_{SI} . Therefore, increasing σ_{ann} (which is allowed in scenarios of non-thermal DM) and keeping σ_{SI} fixed does not enhance the signal from DM annihilation inside the Sun. It only leads to a faster establishment of equilibrium between DM capture and annihilation.

DM annihilation final states that are most relevant for producing neutrinos inside the Sun are prompt neutrinos from H^0/A^0 and H^+/H^- decays, W, Z and τ particles from H^+/H^- and H^{++}/H^{--} decays. Other final states (like e, μ , and lighter quarks) lose their energy and stop almost immediately, which results in production of neutrinos at energies below detection threshold. The charged current interactions inside the Sun convert ν_e, ν_μ, ν_τ to e, μ, τ respectively. Using the charged current neutrino-nucleon cross section [40], we find that neutrino absorption becomes important (i.e., $L_{\text{abs}} < R_C$, with R_C being the core radius of the Sun) at energies $E_\nu > 300 \text{ GeV}$. For ν_e , the flavor and mass eigenstates are the same deep inside the Sun, and hence absorption suppresses the flux of ν_e at energies above 300 GeV. On the other hand, ν_τ absorption produces τ particles that decay quickly before losing too much energy because of very short lifetime of τ . This decay produces ν_τ at a lower energy, and hence this “regeneration” effect populates the spectrum at energies well below the DM mass. Since ν_μ and ν_τ undergo oscillations inside the Sun that is dominantly set by the atmospheric mass splitting Δm_{atm}^2 , we have $L_{\text{osc}} \propto E_\nu / \Delta m_{\text{atm}}^2$. As long as $L_{\text{abs}} \gtrsim L_{\text{osc}}/4$, oscillations mix ν_μ and ν_τ efficiently and ν_μ final states also feel the regeneration effect. When L_{abs} drops below $L_{\text{osc}}/4$, which happens at $E_\nu \sim 500 \text{ GeV}$, oscillations cease to be effective and ν_μ gets absorbed similar to ν_e . As a consequence, only the ν_τ final state retains a significant regeneration signature at energies above 500 GeV.⁹

For neutrinos of sufficiently low energies, vacuum flavor oscillations between the Sun and the Earth are averaged over half a year when the Sun is below the horizon at the south pole. In particular, below 100 GeV, the oscillation length set by the solar mass splitting Δm_{sol}^2 is less than approximately 3 million kilometer change in the Earth-Sun distance over half a year. The situation changes at energies above 100 GeV where solar neutrino oscillations are not averaged out anymore. For monochromatic neutrinos of a single flavor, this significantly affects oscillations between ν_e and ν_μ/ν_τ , and hence the ν_μ spectrum at the detector, at high energies. However, this is not an important effect in our model since DM annihilation produces different neutrino flavors with a continuous energy spectrum in this case.

We use DarkSUSY 5.1.1 [38] to simulate production of neutrinos in the Sun, their propagation to the South Pole, and the interaction of ν_μ with ice at many different energies for all the SM channels. DarkSUSY does this by interpolating an older WimpSim [37] simulation. Here we run WimpSim 3.05 directly for the prompt neutrino channels, sample energies spaced at 10 GeV, and use oscillation parameters found in [54].

We then combine the energy spectra of all the channels at the production point with how they propagate, giving us the final neutrino spectra at the detector.¹⁰ It should be noted that variation of all neutrino oscillation parameters within the 3σ allowed range results in $\mathcal{O}(3 - 4\%)$ change in the final neutrino spectra from the Sun, similar to the Galactic Center case, which is insignificant.

In Fig. 4 we show the spectra of ν_μ at the detector for $v_\Delta = 1 \text{ eV}$ (BP1, BP2) and for $v_\Delta = 1 \text{ GeV}$ (BP3) cases. It is seen that at energies below 400 GeV the NH scenario results in a larger number of ν_μ

⁹Neutrinos also have neutral current interactions with matter inside the Sun that results in energy loss of the neutrinos from all flavors further shifting their spectra toward lower energies. However, the cross section for neutral current interactions is a factor of 3 smaller than that for charged current interactions, which makes them subdominant.

¹⁰Since $\bar{\nu}$ -nucleon cross section is about two times smaller than the ν -nucleon cross section [55, 56], the number of absorbed $\bar{\nu}$ inside the Sun is smaller. This results in a larger $\bar{\nu}$ flux at the detector from DM annihilation inside the Sun.

and eventually muons than the IH scenario. The reason is similar to the Galactic Center case and can be explained by the triplet scalar decay patterns. For $v_\Delta = 1$ eV, as mentioned above, triplet decays mainly produce ν_τ , ν_μ and τ , μ final states in the NH scenario. In the IH scenario, on the other hand, triplet decays mainly produce ν_e and e final states. As far as charged lepton final states are concerned, only τ decays before losing a significant fraction of energy and produces neutrinos. Regarding triplet decays to neutrinos, ν_τ (and to a lesser extent ν_μ) is the most relevant flavor that survive at energies above 300 GeV due to regeneration effect. In consequence, for $v_\Delta = 1$ eV, a larger number of ν_μ arrive at the detector in the NH scenario. However, the neutrino spectra in the two scenarios do not differ when $v_\Delta = 1$ GeV as in earlier case. Comparing the neutrino signal from DM annihilation in

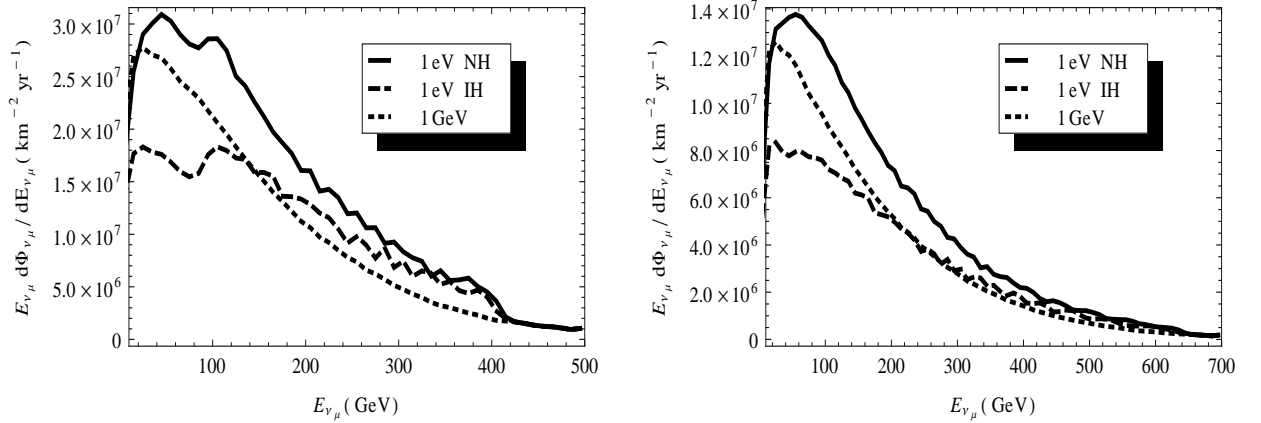


Figure 4: Spectra of ν_μ from DM annihilation inside the Sun at the detector for $m_{\text{DM}} = 500$ GeV (700 GeV) in the left (right) panel.

the Sun (Fig. 4) and at the Galactic Center (Fig. 1), we notice some differences. First, the kinematic cuts in Fig. 1 are not prominent in Fig. 4. This is due to the fact that absorption/regeneration and down scattering inside the Sun erases sharp features in the spectra. More precisely, only a little bump develops at low energies for $m_{\text{DM}} = 500$ GeV due to the boosted triplet scalars, shown in right panel of Fig. 4, unlike the box-like structure that can clearly be observed in the Galactic Center neutrino flux. At higher energies, instead of a bump only the wiggles can be noticed which are the effect of neutrino oscillation. Furthermore, the difference between the spectra in NH and IH scenarios in Fig. 4 is smaller than that in Fig. 1. This is because stopping of muons and partial absorption of ν_μ inside the Sun decreases the overall flux of ν_μ arriving at the detector. Nevertheless, the NH scenario yields a larger flux than the IH scenario when $v_\Delta = 1$ eV.

We emphasize that the neutrino signal from DM annihilation inside the Sun is complementary to that from the Galactic DM annihilation as they are set by different cross sections (σ_{SI} and σ_{ann} respectively). We see from Figs. 1 and 4 that for the model parameters given in Table 1 the signal from the Sun is about an order of magnitude stronger than that from the Galactic Center. As we will discuss later, both of these signals can be enhanced further.

3.3 Muon spectra at the detector

We now present the muon spectra obtained from the conversion of ν_μ at the detector, which is the observed signal at neutrino telescopes. For simulation purpose, we assume a detector that has the same capability as the IceCube DeepCore array. In Fig. 5, we show the spectra of contained and through-going muons in the detector from DM annihilation at the Galactic Center. In this case, the

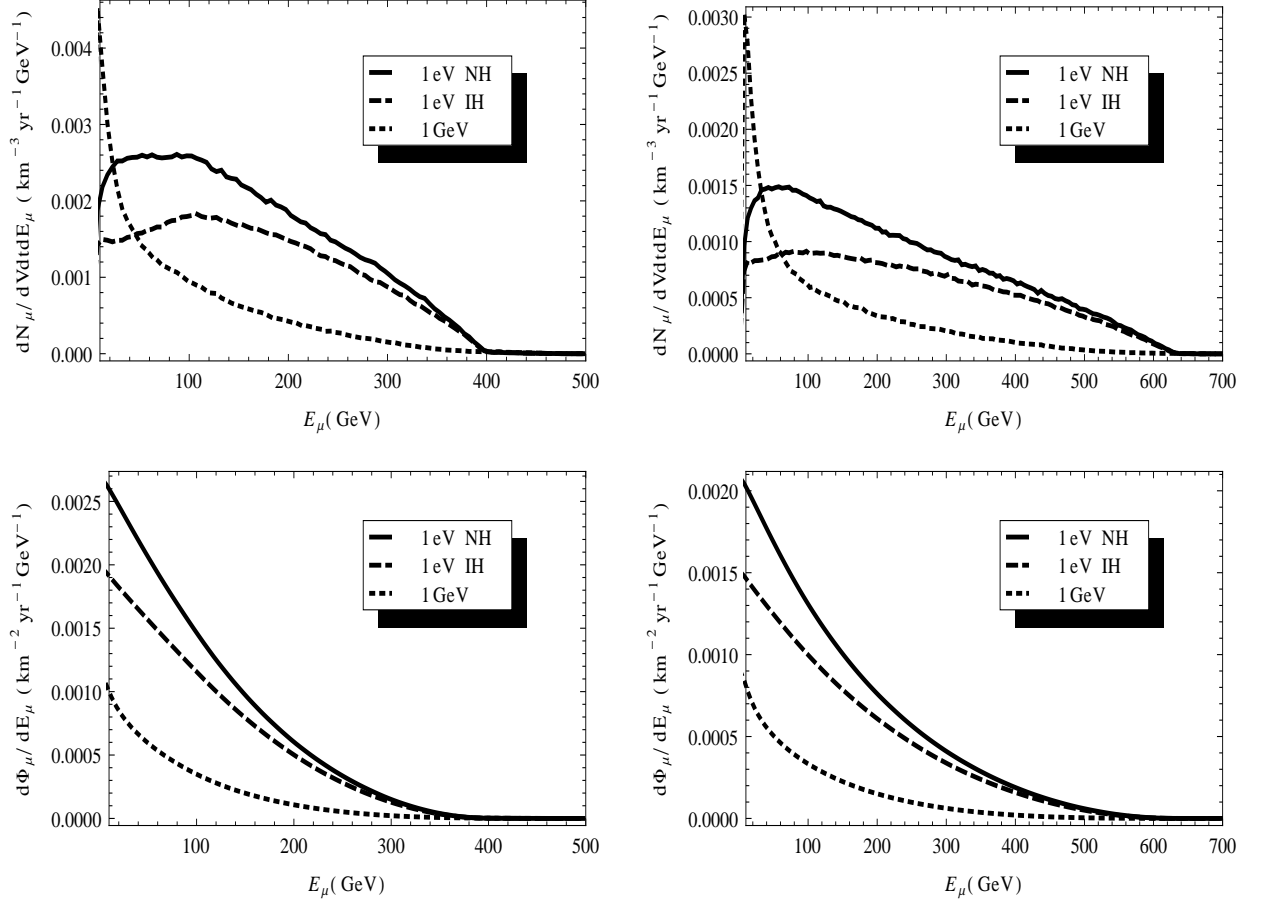


Figure 5: Spectra of muons from DM annihilation at the Galactic Center for $m_{\text{DM}} = 500 \text{ GeV}$ (700 GeV) in the left (right) panel. Upper and lower panels show contained and through-going muon spectra with an angular cut of 5° respectively.

signal comes from a region around the Galactic Center that has 5° angular extension. Hence, in order to optimize the signal to background ratio, we have imposed a 5° angular cut on the muons relative to the center of the galaxy.

In Fig. 6, we show the spectra of contained and through-going muons from DM annihilation inside the Sun. Since the Sun is a point-like source, the optimal signal to background ratio is obtained for an angular cut of 2° , in this case. The peaks in both figures are due to the imposed angular cuts that eliminate muons produced from ν_μ conversion below a certain energy. For through-going muons the peak occurs at a lower energy, which can be understood by noting that the measured energy of a through-going muon is in general less than the actual energy at the production point.

As expected, the muon spectra have less features than the neutrino spectra shown in Figs. 1-4. Nevertheless, the difference between $v_\Delta = 1 \text{ eV}$ and $v_\Delta = 1 \text{ GeV}$ cases, as well as the NH and IH scenarios in the former case, are clearly visible in the muon spectra arising from both the Galactic Center and the Sun. Similar to the neutrino spectra, substantial deviation among the cases is seen in the signal arising from DM annihilation at the Galactic Center than in the Sun. However, we also note that the absolute value of the flux from the Galactic Center is smaller by an order of magnitude than that from the Sun.

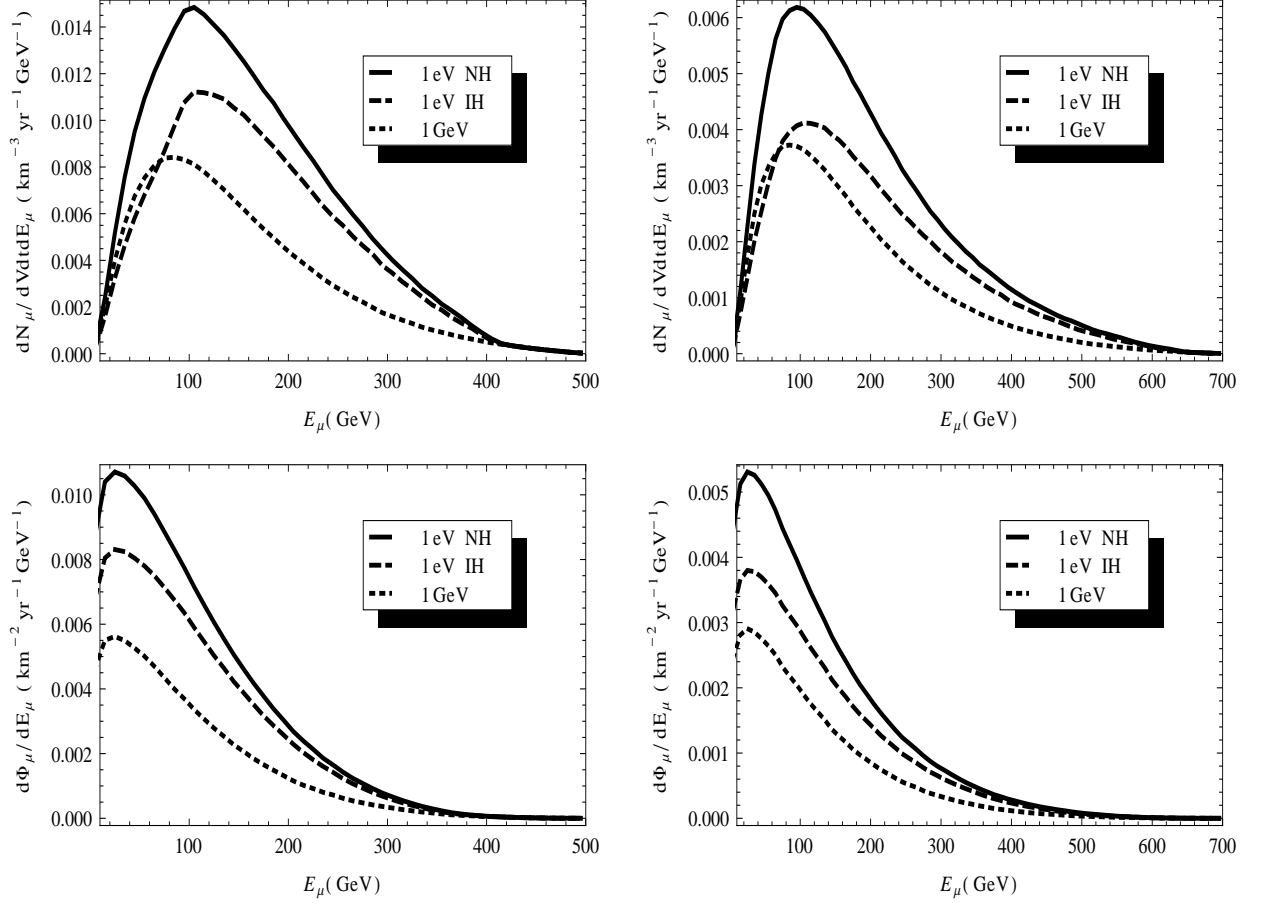


Figure 6: Spectra of muons from DM annihilation in the Sun for $m_{\text{DM}} = 500$ GeV (700 GeV) in the left(right) panel. Upper and lower panels show contained and through-going muon spectra with an angular cut of 2° respectively.

The muon spectra shown in Figs. 5 and 6 are obtained assuming the nominal thermal freeze-out value of $\langle\sigma_{\text{ann}}v\rangle$. However, the Fermi-LAT data from Milky Way dwarf spheroidal galaxies [57] allows larger values on the DM annihilation cross section for the values of DM mass that we have considered here. One can see from Fig. 8 of [57] that for the $b\bar{b}$ and $W^\pm W^\mp$ final states $\langle\sigma_{\text{ann}}v\rangle$ can be larger than the thermal freeze-out value by a factor of 4 (6) when $m_{\text{DM}} = 500$ (700) GeV. In BP1 and BP2, where the distinction between the NH and IH scenarios is significant, these final states arise from DM annihilation to the SM Higgs that is controlled by the coupling λ_Φ of Eq. (3). As explained before, λ_Φ also controls σ_{SI} in our model. Hence raising $\langle\sigma_{\text{ann}}v\rangle$ by the above factors, due to a larger value of λ_Φ , also results in an increase in σ_{SI} compared with that given in Table 1, which is still consistent with the LUX bounds [32]. For the $\tau^+\tau^-$ final state, $\langle\sigma_{\text{ann}}v\rangle$ can be larger than the thermal freeze-out value by a factor of 10 (17) when $m_{\text{DM}} = 500$ (700) GeV¹¹. This final state arises due to DM annihilation to the triplet Higgs, which is controlled by the coupling λ_Δ of Eq. (3). Increasing λ_Δ results in an increase in σ_{ann} , but does not affect σ_{SI} .

Therefore, by invoking non-thermal mechanisms for DM production in the early universe, we can obtain considerably larger neutrino fluxes from DM annihilation at the Galactic Center and inside the Sun.

¹¹ It should be noted that the Fermi-LAT bound cannot be directly applied to our model since we have four-body annihilation final states in this case. Moreover, we have a combination of different final states instead of 100% of just one final state. Nevertheless, the Fermi-LAT limit provides a reasonable upper bound on σ_{ann} in this case too.

The resulting enhancement in the muon events, compared to Figs. 5 and 6, leads to a better prospect for detection of the neutrino signal against the atmospheric background. In Fig. 7, we show the spectra of contained muons due to DM annihilation at the Galactic Center (left panel) and inside the Sun (right panel) for annihilation cross sections that are just below the Fermi-LAT limits, where $m_{\text{DM}} = 500$ GeV and the background from atmospheric neutrinos is also shown for comparison. Contained muons from DM annihilation inside the Sun provide the best detection opportunity. Within energy interval 100-400 GeV, the total number of contained muons for the NH and IH scenarios is 11 and 9 respectively (compared with 95 for the background). The maximum signal to background ratio, 17% and 15% for the NH and IH scenarios respectively, occurs at an energy of 255 GeV. For a neutrino telescope with the same capability as the IceCube DeepCore array, 3σ discovery of NH and IH scenarios takes 8 and 12 years respectively. To distinguish the different neutrino mass hierarchies, one should go beyond the simple number count and perform a careful shape analysis, which is beyond the scope of this paper.

There are proposals for directly measuring the mass hierarchy by using atmospheric neutrinos in future extensions of neutrino telescopes such as PINGU (Precision IceCube Next Generation Upgrade) [58]. It is possible to exclude the wrong mass ordering by this method (as well as in neutrino beam experiments) at the 3σ level within the next 10-15 years [59]. Our approach, which exploits an interesting connection between DM and neutrinos, is complementary to this direct method and makes another case for the future neutrino telescopes with much larger volume like IceCube-Gen2 [60].

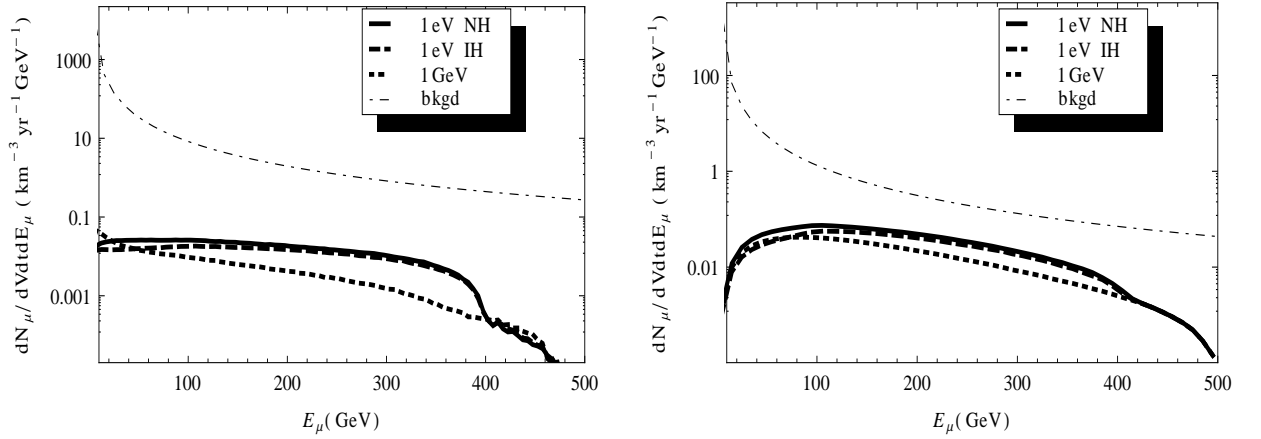


Figure 7: Spectra of contained muons from DM annihilation at the Galactic Center (left) and inside the Sun (right) for $m_{\text{DM}} = 500$ GeV. The value of σ_{ann} used to obtain the muon flux is just below the current bounds from Fermi-LAT. The top line in both figures is due to the background arising from the atmospheric neutrinos.

4 Summary and conclusions

In this paper, we have considered an extension of the SM that explains neutrino masses and mixing angles via the type-II seesaw mechanism and includes a singlet scalar as a viable DM candidate. The DM interacts with the triplet scalar that generates light neutrino masses thereby linking the two sectors. We have studied the neutrino signal from DM annihilation at the Galactic Center and inside the Sun in this model that could be detected at IceCube. Our main results are summarized as follows:

- In the region of the parameter space where the triplet scalar dominantly decays to leptonic final states, the flux of ν_μ from DM annihilation depends upon the neutrino mass hierarchy (normal,

inverted or degenerate). The photon flux, on the other hand, is practically the same for different hierarchies.

- The difference in the flux of ν_μ at the detector for NH and IH is visible. The NH scenario produces a larger flux because of its mass pattern. This holds for both signals from DM annihilation at the Galactic Center and inside the Sun.
- The difference is more significant in the neutrino signal arising from DM annihilation at the Galactic Center than that arises from DM annihilation inside the Sun. This is mainly because the interaction of neutrinos with matter inside the Sun results in a moderate attenuation of the final ν_μ flux at the detector.
- The same reason holds for the contained and through-going muons that are produced from the conversion of ν_μ s at the detector. The muon spectra have less features than the neutrino spectra. Nevertheless, these muons can be detected over the atmospheric background.
- For annihilation cross sections just below the Fermi-LAT limits, future extensions of IceCube are able to discover the neutrino signal and distinguish the different neutrino mass hierarchies with multiyear data.

The LHC in tandem with direct detection experiments, the IceCube and Fermi-LAT will be able to probe this minimal extension of the SM that utilizes a new Higgs sector. Finally, we would like to conclude by pointing out the fact that this analysis can be applied to other models that link DM to the neutrino sector.

5 Acknowledgements

This work is supported in part by NSF Grant No. PHY-1417510 (R.A. and B.K.) and DOE Grant DE-FG02-13ER42020 (B.D.). We thank the International Center for Theoretical Physics (ICTP), Trieste, Italy, where this work was initiated. D.K.G. and I.S. would like to thank Bhupal Dev for useful discussions. D.K.G. also would like to thank Theory Unit of the Physics Department, CERN, Geneva, Switzerland where part of this work was done. R.A. and B.K. would like to thank Shashank Shalgar for valuable discussions. R.A. and B.D. thank the Center for Theoretical Underground Physics and Related Areas (CETUP* 2015) for its hospitality and for partial support during the completion of this work.

Appendix

A Oscillation Probability Calculation

The flavor eigenstate of neutrinos can be related to the mass eigenstate by the 3×3 Pontecorvo-Maki-Nakagawa-Sakata (PMNS) mixing matrix.

$$\begin{pmatrix} \nu_e \\ \nu_\mu \\ \nu_\tau \end{pmatrix} = \begin{pmatrix} U_{e1} & U_{e2} & U_{e3} \\ U_{\mu1} & U_{\mu2} & U_{\mu3} \\ U_{\tau1} & U_{\tau2} & U_{\tau3} \end{pmatrix} \begin{pmatrix} \nu_1 \\ \nu_2 \\ \nu_3 \end{pmatrix} \quad (13)$$

The neutrinos from the Galactic Center encounter flavor oscillation while reaching the Earth. However, since it traverses very large distance with respect to its oscillation length, hence the oscillation term is averaged out. The probability of one neutrino flavor to oscillate into other becomes simply,

$$\langle P(\nu_\alpha \rightarrow \nu_\beta) \rangle = \sum_{i=1}^3 |U_{\alpha_i}|^2 |U_{\beta_i}|^2 \quad (14a)$$

$$= XX^T \quad (14b)$$

with,

$$X = \begin{pmatrix} |U_{e1}|^2 & |U_{e2}|^2 & |U_{e3}|^2 \\ |U_{\mu1}|^2 & |U_{\mu2}|^2 & |U_{\mu3}|^2 \\ |U_{\tau1}|^2 & |U_{\tau2}|^2 & |U_{\tau3}|^2 \end{pmatrix} \quad (14c)$$

The PMNS matrix is usually parametrized in terms of the three mixing angles $\theta_{12}; \theta_{23}; \theta_{13}$, and one Dirac (δ) and two Majorana ($\alpha_1; \alpha_2$) CP phases:

$$U = \begin{pmatrix} c_{12}c_{13} & s_{12}c_{13} & s_{13}e^{-i\delta} \\ -s_{12}c_{23} - c_{12}s_{23}s_{13}e^{i\delta} & c_{12}c_{23} - s_{12}s_{23}s_{13}e^{i\delta} & s_{23}c_{13} \\ s_{12}s_{23} - c_{12}c_{23}s_{13}e^{i\delta} & -c_{12}s_{23} - s_{12}c_{23}s_{13}e^{i\delta} & c_{23}c_{13} \end{pmatrix} \times \text{diag}(e^{i\alpha_1/2}, e^{i\alpha_2/2}, 1) \quad (15)$$

The oscillated flux of the neutrinos at the detector at earth,

$$\begin{pmatrix} \Phi_{\nu_e} \\ \Phi_{\nu_\mu} \\ \Phi_{\nu_\tau} \end{pmatrix} = \begin{pmatrix} P_{11} & P_{12} & P_{13} \\ P_{21} & P_{22} & P_{23} \\ P_{31} & P_{32} & P_{33} \end{pmatrix} \begin{pmatrix} \Phi_{\nu_e}^0 \\ \Phi_{\nu_\mu}^0 \\ \Phi_{\nu_\tau}^0 \end{pmatrix} \quad (16)$$

From Eq. (14b) and Eq. (14c),

$$P_{11} = |U_{e1}|^4 + |U_{e2}|^4 + |U_{e3}|^4 \quad (17a)$$

$$P_{12} = |U_{e1}|^2 |U_{\mu1}|^2 + |U_{e2}|^2 |U_{\mu2}|^2 + |U_{e3}|^2 |U_{\mu3}|^2 = P_{21} \quad (17b)$$

$$P_{13} = |U_{e1}|^2 |U_{\tau1}|^2 + |U_{e2}|^2 |U_{\tau2}|^2 + |U_{e3}|^2 |U_{\tau3}|^2 = P_{31} \quad (17c)$$

$$P_{22} = |U_{\mu1}|^4 + |U_{\mu2}|^4 + |U_{\mu3}|^4 \quad (17d)$$

$$P_{23} = |U_{\mu1}|^2 |U_{\tau1}|^2 + |U_{\mu2}|^2 |U_{\tau2}|^2 + |U_{\mu3}|^2 |U_{\tau3}|^2 = P_{32} \quad (17e)$$

$$P_{33} = |U_{\tau1}|^4 + |U_{\tau2}|^4 + |U_{\tau3}|^4 \quad (17f)$$

We use the latest global analysis of the 3-neutrino oscillation data [54],

$$\begin{aligned} \Delta m_{21}^2 &= 7.60 \times 10^{-5} \text{ eV}^2, & \theta_{12} &= 34.6^\circ, \\ \Delta m_{31}^2 &= 2.48 \times 10^{-3} \text{ eV}^2 \text{ (NH)}, & \Delta m_{31}^2 &= 2.38 \times 10^{-3} \text{ eV}^2 \text{ (IH)}, \\ \delta &= 1.41\pi \text{ (NH)}, & \delta &= 1.48\pi \text{ (IH)}, \\ \theta_{23} &= 48.9^\circ \text{ (NH)}, & \theta_{23} &= 49.2^\circ \text{ (IH)}, \\ \theta_{13} &= 8.6^\circ \text{ (NH)} & \theta_{13} &= 8.7^\circ \text{ (IH)}. \end{aligned} \quad (18)$$

$$\text{Normal Hierarchy : } P = \begin{pmatrix} 0.5380 & 0.1979 & 0.2640 \\ 0.1979 & 0.4240 & 0.3779 \\ 0.2640 & 0.3779 & 0.3579 \end{pmatrix} \quad (19a)$$

$$\text{Inverted Hierarchy : } P = \begin{pmatrix} 0.5377 & 0.2009 & 0.2613 \\ 0.2009 & 0.4223 & 0.3766 \\ 0.2613 & 0.3766 & 0.3620 \end{pmatrix} \quad (19b)$$

References

- [1] G. Jungman, M. Kamionkowski, and K. Griest, *Supersymmetric dark matter*, *Phys.Rept.* **267** (1996) 195–373, [[hep-ph/9506380](#)].
- [2] G. Bertone, D. Hooper, and J. Silk, *Particle dark matter: Evidence, candidates and constraints*, *Phys.Rept.* **405** (2005) 279–390, [[hep-ph/0404175](#)].
- [3] A. Strumia and F. Vissani, *Neutrino masses and mixings and...*, [hep-ph/0606054](#).
- [4] S. F. King, A. Merle, S. Morisi, Y. Shimizu, and M. Tanimoto, *Neutrino Mass and Mixing: from Theory to Experiment*, *New J.Phys.* **16** (2014) 045018, [[arXiv:1402.4271](#)].
- [5] I. Gogoladze, N. Okada, and Q. Shafi, *Type II Seesaw and the PAMELA/ATIC Signals*, *Phys.Lett.* **B679** (2009) 237–241, [[arXiv:0904.2201](#)].
- [6] P. S. B. Dev, D. K. Ghosh, N. Okada, and I. Saha, *Neutrino Mass and Dark Matter in light of recent AMS-02 results*, *Phys.Rev.* **D89** (2014) 095001, [[arXiv:1307.6204](#)].
- [7] R. Allahverdi, S. S. Campbell, B. Dutta, and Y. Gao, *Dark matter indirect detection signals and the nature of neutrinos in the supersymmetric $U(1)_{B-L}$ extension of the standard model*, *Phys.Rev.* **D90** (2014), no. 7 073002, [[arXiv:1405.6253](#)].
- [8] G. Belanger, S. Kraml, and A. Lessa, *Light Sneutrino Dark Matter at the LHC*, *JHEP* **07** (2011) 083, [[arXiv:1105.4878](#)].
- [9] P. S. Bhupal Dev, S. Mondal, B. Mukhopadhyaya, and S. Roy, *Phenomenology of Light Sneutrino Dark Matter in $mSUGRA$ with Inverse Seesaw*, *JHEP* **09** (2012) 110, [[arXiv:1207.6542](#)].
- [10] C. Arina and M. E. Cabrera, *Multi-lepton signatures at LHC from sneutrino dark matter*, *JHEP* **04** (2014) 100, [[arXiv:1311.6549](#)].
- [11] H. An, P. S. B. Dev, Y. Cai, and R. N. Mohapatra, *Sneutrino Dark Matter in Gauged Inverse Seesaw Models for Neutrinos*, *Phys. Rev. Lett.* **108** (2012) 081806, [[arXiv:1110.1366](#)].
- [12] D. K. Ghosh, S. Mondal, and I. Saha, *Confronting the Galactic Center Gamma Ray Excess With a Light Scalar Dark Matter*, *JCAP* **1502** (2015), no. 02 035, [[arXiv:1405.0206](#)].
- [13] M. Lattanzi, R. A. Lineros, and M. Taoso, *Connecting neutrino physics with dark matter*, *New J. Phys.* **16** (2014), no. 12 125012, [[arXiv:1406.0004](#)].
- [14] **IceCube** Collaboration, M. Aartsen et al., *Search for dark matter annihilations in the Sun with the 79-string IceCube detector*, *Phys.Rev.Lett.* **110** (2013), no. 13 131302, [[arXiv:1212.4097](#)].
- [15] **IceCube** Collaboration, M. Aartsen et al., *Search for Dark Matter Annihilation in the Galactic Center with IceCube-79*, [arXiv:1505.07259](#).
- [16] **Fermi-LAT** Collaboration, A. Albert, *Indirect Searches for Dark Matter with the Fermi Large Area Telescope 1*, *Phys.Procedia* **61** (2015) 6–12.
- [17] J. Schechter and J. Valle, *Neutrino Masses in $SU(2) \times U(1)$ Theories*, *Phys.Rev.* **D22** (1980) 2227.
- [18] M. Magg and C. Wetterich, *Neutrino Mass Problem and Gauge Hierarchy*, *Phys.Lett.* **B94** (1980) 61.

- [19] T. Cheng and L.-F. Li, *Neutrino Masses, Mixings and Oscillations in $SU(2) \times U(1)$ Models of Electroweak Interactions*, *Phys.Rev.* **D22** (1980) 2860.
- [20] R. N. Mohapatra and G. Senjanovic, *Neutrino Masses and Mixings in Gauge Models with Spontaneous Parity Violation*, *Phys.Rev.* **D23** (1981) 165.
- [21] G. Lazarides, Q. Shafi, and C. Wetterich, *Proton Lifetime and Fermion Masses in an $SO(10)$ Model*, *Nucl.Phys.* **B181** (1981) 287–300.
- [22] P. Fileviez Perez, T. Han, G.-y. Huang, T. Li, and K. Wang, *Neutrino Masses and the CERN LHC: Testing Type II Seesaw*, *Phys.Rev.* **D78** (2008) 015018, [[arXiv:0805.3536](#)].
- [23] A. Melfo, M. Nemevsek, F. Nesti, G. Senjanovic, and Y. Zhang, *Type II Seesaw at LHC: The Roadmap*, *Phys.Rev.* **D85** (2012) 055018, [[arXiv:1108.4416](#)].
- [24] **Particle Data Group** Collaboration, K. Olive et al., *Review of Particle Physics*, *Chin.Phys.* **C38** (2014) 090001.
- [25] F. del Aguila, J. Aguilar-Saavedra, J. de Blas, and M. Perez-Victoria, *Electroweak constraints on see-saw messengers and their implications for LHC*, [arXiv:0806.1023](#).
- [26] A. Akeroyd, M. Aoki, and H. Sugiyama, *Lepton Flavour Violating Decays $\tau \rightarrow \text{anti-}l \ell$ and $\mu \rightarrow e \gamma$ in the Higgs Triplet Model*, *Phys.Rev.* **D79** (2009) 113010, [[arXiv:0904.3640](#)].
- [27] T. Fukuyama, H. Sugiyama, and K. Tsumura, *Constraints from muon $g-2$ and LFV processes in the Higgs Triplet Model*, *JHEP* **1003** (2010) 044, [[arXiv:0909.4943](#)].
- [28] S. Kanemura and K. Yagyu, *Radiative corrections to electroweak parameters in the Higgs triplet model and implication with the recent Higgs boson searches*, *Phys. Rev.* **D85** (2012) 115009, [[arXiv:1201.6287](#)].
- [29] P. Bhupal Dev, D. K. Ghosh, N. Okada, and I. Saha, *125 GeV Higgs Boson and the Type-II Seesaw Model*, *JHEP* **1303** (2013) 150, [[arXiv:1301.3453](#)].
- [30] **Planck** Collaboration, P. Ade et al., *Planck 2013 results. XVI. Cosmological parameters*, *Astron.Astrophys.* **571** (2014) A16, [[arXiv:1303.5076](#)].
- [31] **ATLAS** Collaboration, G. Aad et al., *Search for anomalous production of prompt same-sign lepton pairs and pair-produced doubly charged Higgs bosons with $\sqrt{s} = 8$ TeV pp collisions using the ATLAS detector*, *JHEP* **03** (2015) 041, [[arXiv:1412.0237](#)].
- [32] **LUX** Collaboration, D. Akerib et al., *First results from the LUX dark matter experiment at the Sanford Underground Research Facility*, *Phys.Rev.Lett.* **112** (2014) 091303, [[arXiv:1310.8214](#)].
- [33] J. D. Barrow, *MASSIVE PARTICLES AS A PROBE OF THE EARLY UNIVERSE*, *Nucl. Phys.* **B208** (1982) 501–508.
- [34] J. McDonald, *WIMP Densities in Decaying Particle Dominated Cosmology*, *Phys. Rev.* **D43** (1991) 1063–1068.
- [35] M. Kamionkowski and M. S. Turner, *THERMAL RELICS: DO WE KNOW THEIR ABUNDANCES?*, *Phys. Rev.* **D42** (1990) 3310–3320.
- [36] M. Honda, T. Kajita, K. Kasahara, S. Midorikawa, and T. Sanuki, *Calculation of atmospheric neutrino flux using the interaction model calibrated with atmospheric muon data*, *Phys.Rev.* **D75** (2007) 043006, [[astro-ph/0611418](#)].

- [37] M. Blennow, J. Edsjo, and T. Ohlsson, *Neutrinos from WIMP annihilations using a full three-flavor Monte Carlo*, *JCAP* **0801** (2008) 021, [[arXiv:0709.3898](#)].
- [38] P. Gondolo, J. Edsjo, P. Ullio, L. Bergstrom, M. Schelke, et al., *DarkSUSY: Computing supersymmetric dark matter properties numerically*, *JCAP* **0407** (2004) 008, [[astro-ph/0406204](#)].
- [39] C. Andreopoulos, A. Bell, D. Bhattacharya, F. Cavanna, J. Dobson, et al., *The GENIE Neutrino Monte Carlo Generator*, *Nucl.Instrum.Meth.* **A614** (2010) 87–104, [[arXiv:0905.2517](#)].
- [40] E. K. Akhmedov, S. Razzaque, and A. Y. Smirnov, *Mass hierarchy, 2-3 mixing and CP-phase with Huge Atmospheric Neutrino Detectors*, *JHEP* **1302** (2013) 082, [[arXiv:1205.7071](#)].
- [41] D. Chirkin and W. Rhode, *Muon Monte Carlo: A High-precision tool for muon propagation through matter*, [hep-ph/0407075](#).
- [42] A. Alloul, N. D. Christensen, C. Degrande, C. Duhr, and B. Fuks, *FeynRules 2.0 - A complete toolbox for tree-level phenomenology*, *Comput.Phys.Commun.* **185** (2014) 2250–2300, [[arXiv:1310.1921](#)].
- [43] A. Belyaev, N. D. Christensen, and A. Pukhov, *CalcHEP 3.4 for collider physics within and beyond the Standard Model*, *Comput.Phys.Commun.* **184** (2013) 1729–1769, [[arXiv:1207.6082](#)].
- [44] T. Sjostrand, S. Mrenna, and P. Z. Skands, *PYTHIA 6.4 Physics and Manual*, *JHEP* **0605** (2006) 026, [[hep-ph/0603175](#)].
- [45] G. Belanger, F. Boudjema, A. Pukhov, and A. Semenov, *micrOMEGAs4.1: two dark matter candidates*, [arXiv:1407.6129](#).
- [46] J. F. Navarro, C. S. Frenk, and S. D. White, *The Structure of cold dark matter halos*, *Astrophys.J.* **462** (1996) 563–575, [[astro-ph/9508025](#)].
- [47] Y. Zeldovich, A. Klypin, M. Y. Khlopov, and V. Chechetkin, *Astrophysical constraints on the mass of heavy stable neutral leptons*, *Sov.J.Nucl.Phys.* **31** (1980) 664–669.
- [48] J. Silk, K. A. Olive, and M. Srednicki, *The Photino, the Sun and High-Energy Neutrinos*, *Phys.Rev.Lett.* **55** (1985) 257–259.
- [49] L. M. Krauss, K. Freese, W. Press, and D. Spergel, *Cold dark matter candidates and the solar neutrino problem*, *Astrophys.J.* **299** (1985) 1001.
- [50] L. M. Krauss, M. Srednicki, and F. Wilczek, *Solar System Constraints and Signatures for Dark Matter Candidates*, *Phys.Rev.* **D33** (1986) 2079–2083.
- [51] W. H. Press and D. N. Spergel, *Capture by the sun of a galactic population of weakly interacting massive particles*, *Astrophys.J.* **296** (1985) 679–684.
- [52] T. Gaisser, G. Steigman, and S. Tilav, *Limits on Cold Dark Matter Candidates from Deep Underground Detectors*, *Phys.Rev.* **D34** (1986) 2206.
- [53] V. Barger, Y. Gao, and D. Marfatia, *Dark matter at DeepCore and IceCube*, *Phys.Rev.* **D83** (2011) 055012, [[arXiv:1101.4410](#)].
- [54] D. V. Forero, M. Tortola, and J. W. F. Valle, *Neutrino oscillations refitted*, *Phys. Rev.* **D90** (2014), no. 9 093006, [[arXiv:1405.7540](#)].

- [55] R. Gandhi, C. Quigg, M. H. Reno, and I. Sarcevic, *Ultrahigh-energy neutrino interactions*, *Astropart. Phys.* **5** (1996) 81–110, [[hep-ph/9512364](#)].
- [56] A. Cooper-Sarkar and S. Sarkar, *Predictions for high energy neutrino cross-sections from the zeus global pdf fits*, *JHEP* **01** (2008) 075, [[arXiv:0710.5303](#)].
- [57] **Fermi-LAT** Collaboration, M. Ackermann et al., *Searching for Dark Matter Annihilation from Milky Way Dwarf Spheroidal Galaxies with Six Years of Fermi-LAT Data*, [arXiv:1503.02641](#).
- [58] **IceCube PINGU** Collaboration, D. F. Cowen, T. DeYoung, D. Grant, D. A. Dwyer, S. R. Klein, K. B. Luk, and D. R. Williams, *Measuring the Neutrino Mass Hierarchy with Atmospheric Neutrinos*, [arXiv:1409.5755](#).
- [59] M. Blennow, P. Coloma, P. Huber, and T. Schwetz, *Quantifying the sensitivity of oscillation experiments to the neutrino mass ordering*, *JHEP* **03** (2014) 028, [[arXiv:1311.1822](#)].
- [60] **IceCube** Collaboration, M. G. Aartsen et al., *IceCube-Gen2: A Vision for the Future of Neutrino Astronomy in Antarctica*, [arXiv:1412.5106](#).